

Event Detection for Parameter-to-KPI Dependency Learning for AI-RAN

Christie Djidjev
Idaho National Laboratory
Idaho Falls, United States
Christie.Djidjev@inl.gov

Nicholas Kaminski
Idaho National Laboratory
Idaho Falls, United States
Nicholas.Kaminski@inl.gov

Abstract—Next-generation wireless networks are expected to rely on multiple concurrent AI-driven control functions that optimize different network objectives simultaneously, particularly in AI-integrated and open radio access network architectures such as AI Radio Access Network (AI-RAN) and Open Radio Access Network (O-RAN). When these functions interact, they can interfere with one another in ways that are difficult to detect from raw network data alone. A key missing piece for managing such interactions is a reliable, interpretable dependency structure that captures which control parameters are actively influencing which network performance outcomes at any given time. This paper focuses on the event-detection step needed to support such dependency learning: converting noisy continuous telemetry into binary indicators of parameter activity and KPI response. The central difficulty is that not every fluctuation in the data reflects a genuine control interaction, so the method must distinguish real parameter–outcome relationships from background variation. Because real AI-RAN traffic traces with known parameter–KPI ground truth are difficult to obtain, we introduce a synthetic closed-loop traffic generator with planted latent dependencies. We use this controlled telemetry to evaluate a machine-learning-based dependency recovery pipeline that formulates the conversion of continuous traces into binary event indicators as a significance-detection problem. Experimental evaluation shows that the proposed pipeline reliably recovers the latent dependency structure from noisy continuous traces when the signal is sufficiently separated from background variation, while highlighting threshold calibration as the key factor controlling event-detection quality. These results constitute a foundational step toward interpretable dependency learning toward adaptive AI-RAN control systems.

Index Terms—AI-RAN, O-RAN, Boolean inference, dependency learning, interpretable machine learning, synthetic RAN traffic generation.

I. INTRODUCTION

Modern cellular networks are moving toward AI-enabled, distributed, and programmable control, where multiple control functions may be instantiated across different RAN components, management layers, and timescales. These functions may adjust network parameters for objectives such as mobility management, load balancing, interference control, slicing, and resource optimization. As control becomes more automated and data-driven, the behavior of the overall network is determined not only by each function in isolation, but also by how their actions interact through shared parameters, shared network elements, and overlapping key performance indicators (KPIs).

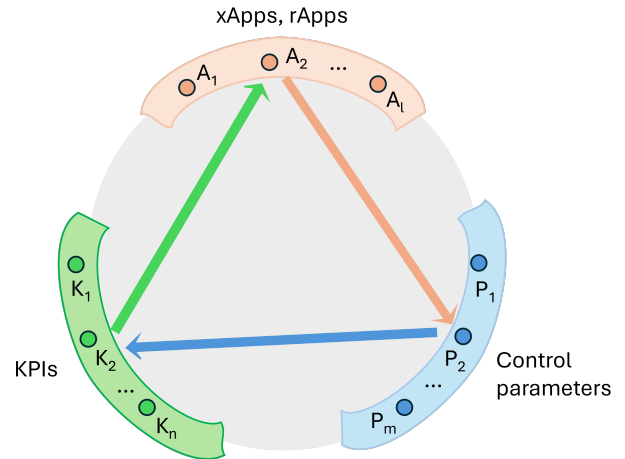


Fig. 1. Information flow between control applications, control parameters, and KPIs in AI-RAN/O-RAN. Multiple control functions, such as xApps and rApps, update network control parameters to meet performance objectives. These parameters, together with external events, influence the observed KPIs. The observed KPIs are then fed back to the applications and influence subsequent control decisions.

This multi-control-point setting is already visible in contemporary cellular architectures. For example, 5G NG-RAN separates centralized and distributed RAN functions through the gNB-CU/gNB-DU split, while open and programmable RAN architectures expose additional control points and interfaces through components such as the Near-RT RIC, Non-RT RIC, O-CU, O-DU, and O-RU [1]–[4]. These architectural trends create an important opportunity: specialized control functions can be developed independently and combined to improve network behavior. At the same time, they create a systems problem: when multiple independently developed control functions act in the same network, their interactions can no longer be understood only from the design of any one function in isolation [5]–[9].

Fig. 1 illustrates this basic feedback setting: multiple control applications update network control parameters, those parameters influence observed KPIs, and KPI observations then feed back into future control decisions. This work studies the problem of learning compact parameter-to-KPI dependency representations from noisy continuous telemetry.

This challenge becomes even more important in the tran-

sition to AI-RAN. While open and programmable RAN architectures make multi-point control more modular, AI-RAN pushes this further by embedding artificial intelligence more deeply into monitoring, prediction, and control, so that network decisions become increasingly adaptive and data-driven rather than fixed in advance [10], [11]. As a result, the network is no longer just running multiple control applications; it is running multiple control applications whose behavior may evolve with data, context, and operating conditions. This makes the overall system more capable, but also harder to reason about. Relationships between control parameters and key performance indicators (KPIs) may be hidden, dynamic, and scenario-dependent, and conflicts between control functions may emerge even when each function appears well behaved on its own. Prior O-RAN conflict work has shown that direct conflicts may be visible before deployment, while indirect and implicit conflicts are much harder to identify because they depend on nontrivial parameter–KPI relationships that are not always known in advance [5]–[9].

These observations motivate the central problem considered in this paper: how to learn and track an interpretable dependency structure that captures which control parameters meaningfully affect which KPIs in the current operating regime. Such a dependency structure is useful because it provides a compact representation of how the system is behaving internally, and because it can support downstream tasks such as conflict analysis, monitoring, and mitigation. However, this structure is not directly visible in raw telemetry. Parameters and KPIs are observed as continuous, noisy time series, and small fluctuations may reflect measurement noise, background variation, or benign adaptation rather than meaningful control influence. Recovering a useful dependency model therefore requires more than simply thresholding telemetry or fitting a black-box predictor: it requires constructing an interpretable representation that preserves the support of the true parameter–KPI relationships while remaining usable in a live control setting. This perspective is consistent with downstream runtime formulations that use a binary dependency matrix as an input representation [12]. This paper focuses on learning such parameter-to-KPI dependencies from noisy telemetry.

A key practical issue is timescale. The separation between slower model learning and faster runtime control follows an established design principle in both programmable RAN architectures and two-timescale control. In O-RAN, the Near-RT RIC supports near-real-time control and optimization on the order of 10 ms–1 s, while the Non-RT RIC supports longer-horizon optimization, policy guidance, and AI/ML model training and updates for Near-RT functions [2]–[4]. More generally, two-timescale stochastic approximation and singular-perturbation control analyze systems in which fast variables evolve while slow variables are treated as approximately fixed, and slow variables are updated using aggregate information from the fast dynamics [13]–[15]. We therefore use this established fast/slow separation as the architectural motivation for our learning-loop formulation, applying the idea to the problem of refreshing parameter–KPI dependency models in

AI-RAN.

In our setting, the slow loop performs telemetry analysis, significance detection, Booleanization, and dependency-model refresh, while the fast loop uses the resulting compact Boolean dependency representation for lightweight runtime reasoning. This separation is useful because rich ML/AI analysis can uncover hidden parameter–KPI structure, but such analysis is typically too heavy and less transparent for direct placement in the fast operational path. The resulting binary dependency layer therefore acts as the interface between slow data-driven learning and fast interpretable reasoning.

The goal is to learn an interpretable dependency layer that can be refreshed from noisy telemetry and then supplied to a fast loop. Concretely, we study how to recover a binary parameter–KPI dependency structure from continuous traces in a way that is robust to noise and suitable for operational use. A key premise of this paper is that converting continuous telemetry into a Boolean abstraction is not merely a preprocessing step, but a central component of interpretable dependency recovery, consistent with broader work on event detection, anomaly detection, and time-series monitoring [12], [16]–[22].

A further challenge is evaluation: in operational AI-RAN telemetry, parameter updates and KPI trajectories may be observable, but the true latent parameter–KPI dependency structure is generally not labeled, making it difficult to directly measure support-recovery accuracy; following standard practice in time-series structure-learning benchmarks, where model-based data-generating processes with known ground-truth graphs are used for quantitative evaluation, we construct a closed-loop AI-RAN-inspired data-generating model with planted parameter–KPI dependencies to isolate the dependency-recovery problem and evaluate whether the proposed Booleanization step preserves the information needed for downstream reasoning [23].

The main contributions of this paper are as follows:

- 1) Motivated by established fast/slow control architectures, we formulate quantized parameter–KPI dependency learning as a slow-loop model-refresh problem, where telemetry analysis supplies a compact interpretable representation for fast runtime reasoning.
- 2) We instantiate a controlled, model-based closed-loop benchmark for AI-RAN dependency recovery, with planted parameter–KPI dependencies and tunable noise/intervention regimes, enabling controlled evaluation of whether the proposed Booleanization pipeline preserves recoverable dependency structure.
- 3) Building on the fast/slow framing in Contribution 1 and the controlled benchmark in Contribution 2, we develop a data-driven event-detection procedure that converts continuous telemetry into a binary parameter–KPI dependency representation that can be periodically refreshed to support tracking of changing relationships over time.
- 4) We verify that the controlled telemetry contains recoverable parameter–KPI structure and quantify how signal

strength, detector threshold, and dependency complexity affect the quality of the learned binary event representation.

II. METHODS

This section describes the methodology used to study interpretable parameter–KPI dependency learning. We first construct synthetic AI-RAN-like telemetry with a known latent dependency structure. We then verify, before any binary event abstraction is applied, that these continuous traces contain enough information to recover the underlying support structure. Finally, we convert the continuous traces into binary activity and response events through a data-driven significance-detection procedure, which we refer to as Booleanization. The overall goal is not to model every detail of an AI-RAN deployment, but to isolate the core question of this paper: whether noisy continuous telemetry can be converted into a compact Boolean dependency representation that remains interpretable and useful for downstream reasoning.

A. Data Generation

To create the controlled setting needed for dependency-recovery evaluation, we construct a model-based closed-loop data-generating process for AI-RAN-like telemetry over a set of controllable parameters and observable KPIs, while keeping the underlying parameter–KPI dependency structure known. Specifically, we model n_P control parameters $P_i(t)$, $i = 1, \dots, n_P$, and n_K KPIs $K_j(t)$, $j = 1, \dots, n_K$, observed over discrete timesteps $t = 0, \dots, T$. The generator is based on a simple closed-loop picture that is natural for many AI-RAN control applications: xApps or rApps observe KPI values, compare them against desired operating regions, and modify control parameters when those KPIs drift too far from their preferred ranges. This is not intended as a universal model of all xApps or rApps, since some applications optimize long-horizon objectives or use more complex policies. However, it is representative of a broad and important class of feedback-driven control functions in which KPI deviations trigger corrective parameter updates.

The latent parameter–KPI structure is encoded by a binary matrix $L^* \in \{0, 1\}^{n_K \times n_P}$, where $L_{j,i}^* = 1$ means that parameter P_i can affect KPI K_j , and $L_{j,i}^* = 0$ means that it cannot. Thus, each row of L^* specifies which parameters are capable of influencing a given KPI. We also associate a sign matrix $S \in \{-1, 0, 1\}^{n_K \times n_P}$ with these dependencies, where $S_{j,i}$ indicates whether increasing parameter P_i tends to push KPI K_j upward or downward whenever $L_{j,i}^* = 1$. Together, L^* and S define the hidden control structure that the learning procedure is ultimately expected to recover.

Each KPI K_j is assigned a preferred operating interval $[K_{j,\text{pref}}^{\min}, K_{j,\text{pref}}^{\max}]$. When a KPI remains inside that interval, the controller has no strong reason to intervene, and the system evolves mainly through background variation. When a KPI moves outside its preferred range, the generator changes the connected parameters by fixed increments and then updates the KPIs accordingly. Because each update is based on the current

system state, the resulting traces form a temporally consistent sequence rather than a collection of unrelated states.

Schematically, the synthetic process can be viewed as

$$P_i(t+1) = P_i(t) + u_i(t+1), \quad (1)$$

$$K_j(t+1) = K_j(t) + \sum_{i=1}^{n_P} L_{j,i}^* S_{j,i} u_i(t+1) + \eta_j(t+1), \quad (2)$$

where $u_i(t+1)$ denotes the control-driven increment applied to parameter P_i , and $\eta_j(t+1)$ captures exogenous variation that can change KPI K_j independently of the modeled parameter updates. The equation in (2) is meant as an intuitive summary of the generator rather than a claim that operational AI-RAN dynamics are exactly linear. The key point is that KPI increments are generated from parameter increments through a known hidden support pattern L^* , while the KPI side is perturbed by unmodeled external effects. Although we focus on the linear form here for clarity, the same estimation and tracking ideas should extend naturally to a broader class of parameter-to-KPI dependencies, particularly when those dependencies are continuous and monotone. Such generalizations are left for follow-up work.

This construction yields several features that are important for the rest of the paper. First, dependencies can overlap: multiple parameters may affect the same KPI, and a single parameter may affect multiple KPIs. Second, the effect of a parameter update depends on the current KPI state, because the controller intervenes only when a KPI falls outside its preferred range. Third, the generator records both absolute trajectories $(P(t), K(t))$ and incremental traces $(\Delta P(t), \Delta K(t))$. The incremental view is particularly useful later, when changes are converted into event indicators for dependency learning.

These behaviors are controlled by a small set of generator settings. The main ones are the dependency matrix $L^* \in \{0, 1\}^{n_K \times n_P}$, the sign matrix $S \in \{-1, 0, 1\}^{n_K \times n_P}$, the intervention step size ΔP_{step} , the preferred KPI intervals $\{[K_{j,\text{pref}}^{\min}, K_{j,\text{pref}}^{\max}]\}_{j=1}^{n_K}$, the trajectory length T , the KPI-variation scale σ , and the number of starting points n_{start} . Structural properties such as sparsity and overlap are determined by the choice of L^* rather than introduced as separate parameters. Among these settings, the most important for the later Booleanization stage is the balance between ΔP_{step} and σ , since this determines how easily meaningful KPI responses can be separated from background fluctuations.

B. Recovering the latent support from continuous traces

Before introducing the Boolean conversion algorithm, we first ask whether the latent dependency structure L^* is already recoverable from the continuous traces. This subsection serves as a verification step for both the generator and the overall learning problem. If a simple interpretable model can recover the planted support pattern from $(\Delta P, P, K)$ and ΔK , then the synthetic data do in fact contain the structure we want to study. This check is especially important because the later Booleanization step replaces the continuous traces by a coarser event-level representation and thus necessarily discards

information. If the latent support is not recoverable with sufficient accuracy in the continuous setting, then it is unlikely to be recovered more reliably by algorithms that operate only on Booleanized data. Recoverability from continuous traces therefore serves as an important verification step before introducing the Boolean abstraction.

To carry out this check, we use decision trees as predictive models, chosen for their interpretability in the continuous setting. For each KPI K_j , we define a supervised prediction problem in which the input at time t is

$$x(t) = \Delta P_1(t), \dots, \Delta P_{n_P}(t), \\ P_1(t), \dots, P_{n_P}(t), K_1(t), \dots, K_{n_K}(t), \quad (3)$$

and the target is

$$y_j(t) = \Delta K_j(t).$$

To train the tree as an interpretable classifier, we replace the continuous target $y_j(t)$ with a discretized label

$$\tilde{y}_j(t) = Q(\Delta K_j(t)),$$

where $Q(\cdot)$ maps each KPI increment to the nearest value in the discrete set

$$V = \{-2\Delta P_{\text{step}}, -\Delta P_{\text{step}}, 0, \Delta P_{\text{step}}, 2\Delta P_{\text{step}}\}.$$

Thus, $\tilde{y}_j(t)$ records which canonical signed increment is closest to the observed $\Delta K_j(t)$. In the experiments reported here, $\Delta P_{\text{step}} = 5$, so the discrete target values are $\{-10, -5, 0, 5, 10\}$. For readability in the tree diagrams, we denote these five classes symbolically by $\{-, -, =, +, ++\}$, corresponding respectively to $\{-10, -5, 0, 5, 10\}$. This preserves more information than a pure change/no-change label while still allowing the use of an interpretable classifier.

The verification procedure has three main stages. First, for each KPI K_j , we train a decision tree to predict its discretized increment from the current system state and the current parameter changes. Second, for each pair (K_j, P_i) , we inspect the learned tree for K_j and count how many nonredundant splits occur on the feature ΔP_i ; we denote this count by $N(K_j, P_i)$. Third, we aggregate these counts across all KPI–parameter pairs to construct an estimated binary dependency matrix L_{pred} .

1) *Decision-tree prediction of KPI increments:* For each KPI K_j , we train a separate decision-tree model using the input–target pairs $(x(t), \tilde{y}_j(t))$ defined above. Including both ΔP and the absolute state variables (P, K) serves a specific purpose. The ΔP features describe what control action was taken at the current step, while the P and K features describe the operating regime in which that action occurred. Together, these features allow the decision tree to model KPI dynamics from the continuous state rather than trying to infer L^* from parameter changes alone.

2) *Counting nonredundant parameter splits:* After one decision tree has been trained for each KPI, the second stage inspects the learned trees to quantify evidence of dependency. The key idea is that a parameter should be counted as influential for KPI K_j only if the tree for K_j uses the corresponding

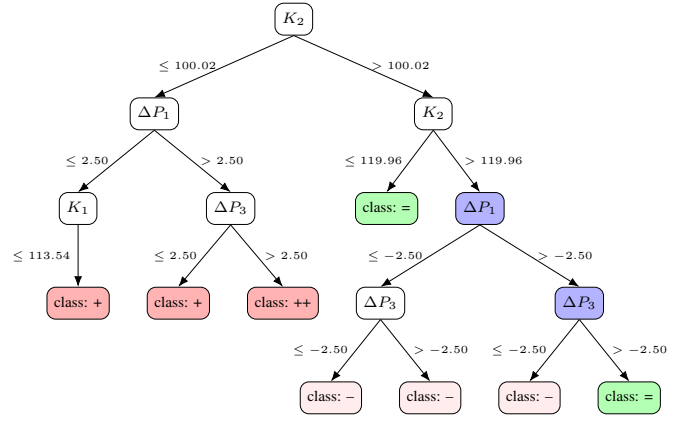


Fig. 2. Example learned decision tree for ΔK_2 . Leaves output discretized classes, shown symbolically as $\{-, -, =, +, ++\}$, corresponding respectively to the target values $\{-10, -5, 0, 5, 10\}$. Leaf colors distinguish prediction classes, while blue internal nodes mark parameter-increment splits that are treated as evidence of dependency because their branches can lead to different downstream predicted classes.

increment feature ΔP_i in a way that actually changes the model’s downstream prediction. A mere appearance of ΔP_i in the tree is not enough, since a tree may contain a split that partitions the data without changing the predicted outcome. Figure 2 illustrates this criterion.

Accordingly, for a fixed KPI K_j and parameter P_i , we inspect all tree nodes that split on ΔP_i . A split is counted as nonredundant if its two child subtrees can lead to different downstream predictions for ΔK_j . We denote by $N(K_j, P_i)$ the number of such nonredundant splits in the tree trained for KPI K_j .

3) *Stage 3: Constructing the estimated support matrix:* In the third stage, we convert the counts $N(K_j, P_i)$ into an estimated binary dependency matrix L_{pred} . For each KPI–parameter pair (K_j, P_i) , we declare an influence to be present if the corresponding tree contains at least one nonredundant split on ΔP_i . Formally, we define

$$L_{\text{pred}}[j, i] = \begin{cases} 1, & \text{if } N(K_j, P_i) \geq 1, \\ 0, & \text{otherwise.} \end{cases}$$

This aggregation yields an interpretable recoverability test: $L_{\text{pred}}[j, i] = 1$ if and only if the tree for K_j contains at least one nonredundant split on ΔP_i .

C. Booleanization by significance detection

Given continuous traces $\Delta P_i(t)$ and $\Delta K_j(t)$, the problem we consider here is to identify which parameter changes and KPI changes are significant enough to be attributed to control activity rather than to background variation or external effects. In other words, we seek a binary representation that retains meaningful control-related events while suppressing fluctuations that do not reflect actionable parameter–KPI interactions.

This objective differs from that of the previous subsection. There, the goal was to verify whether the latent dependency structure is recoverable from the continuous traces themselves.

Here, the goal is to convert those continuous traces into binary event indicators for parameter activity and KPI response. The resulting Boolean traces can then be used in a subsequent support-inference procedure to recover the binary parameter–KPI dependency matrix and to enable real-time conflict detection and prediction, which is one of the main goals stated in the introduction.

By (1) and (2),

$$\Delta P_i(t) = u_i(t), \quad \Delta K_j(t) = \sum_{i=1}^{n_P} L_{j,i}^* S_{j,i} \Delta P_i(t) + \eta_j(t),$$

where $u_i(t+1)$ denotes the control-driven increment applied to parameter P_i and $\eta_j(t)$ denotes the external KPI variation not explained by the modeled control update.

We now Booleanize both the parameter and KPI increments. On the parameter side, the goal is to construct a binary activity indicator

$$B_P(i, t) \in \{0, 1\}$$

that records whether parameter P_i underwent a meaningful update at timestep t . In the current generator, parameter updates are discrete control actions rather than noisy measurements, so we do not introduce a separate noise term on the P -side. Accordingly, the present implementation defines

$$B_P(i, t) = \begin{cases} 1, & \text{if } \Delta P_i(t) \neq 0, \\ 0, & \text{if } \Delta P_i(t) = 0. \end{cases}$$

Thus, a null row is a timestep at which $B_P(i, t) = 0$ for all i , equivalently, a timestep at which all parameter increments are zero.

On the KPI side, the goal is to construct a binary response indicator

$$B_K(j, t) \in \{0, 1\}$$

that records whether KPI K_j exhibits a significant response at timestep t . Unlike the parameter side, this is not immediate, because even when no control action occurs, $\Delta K_j(t)$ may still vary because of external events. We therefore estimate a KPI-specific no-update baseline from null rows, i.e., timesteps at which no parameter update occurs. Formally, let

$$\mathcal{T}_0 = \left\{ t : \sum_{i=1}^{n_P} |\Delta P_i(t)| = 0 \right\}$$

denote the set of null rows. For each KPI K_j , we collect the null-row increments

$$\{\Delta K_j(t) : t \in \mathcal{T}_0\},$$

and estimate the null baseline parameters by

$$\hat{\mu}_j = \frac{1}{|\mathcal{T}_0|} \sum_{t \in \mathcal{T}_0} \Delta K_j(t),$$

$$\hat{\sigma}_j = \max \left\{ \sqrt{\frac{1}{|\mathcal{T}_0| - 1} \sum_{t \in \mathcal{T}_0} (\Delta K_j(t) - \hat{\mu}_j)^2}, 10^{-8} \right\}.$$

TABLE I
RECOVERABILITY OF THE LATENT DEPENDENCY STRUCTURE FROM
CONTINUOUS TRACES BEFORE BOOLEANIZATION.

Condition	Precision	Recall	F1	Exact-match accuracy
Overall	0.980 ± 0.103	0.975 ± 0.120	0.975 ± 0.108	0.946 ± 0.155
Sparse	0.958 ± 0.200	0.958 ± 0.200	0.958 ± 0.200	0.980 ± 0.097
Moderate overlap	0.987 ± 0.070	0.983 ± 0.095	0.982 ± 0.080	0.961 ± 0.137
High overlap	0.983 ± 0.049	0.973 ± 0.086	0.975 ± 0.059	0.908 ± 0.191

We then standardize each KPI increment as

$$z_j(t) = \frac{\Delta K_j(t) - \hat{\mu}_j}{\hat{\sigma}_j},$$

and declare a significant KPI response when

$$B_K(j, t) = \mathbf{1}\{|z_j(t)| > z_{\text{th}}\}, \quad (4)$$

where z_{th} is a fixed tunable threshold.

Algorithmically, the procedure for the KPIs has three steps: first identify the null rows \mathcal{T}_0 from timesteps with no parameter update; second estimate $\hat{\mu}_j$ and $\hat{\sigma}_j$ for each KPI from the corresponding null-row increments; third compute the z-scores $z_j(t)$ and threshold them to obtain $B_K(j, t)$. Together with the observed parameter increments, these binary KPI-response indicators provide the event representation used in the downstream dependency-inference stage.

III. EXPERIMENTAL RESULTS AND DISCUSSION

This section evaluates the main stages of the proposed learning-loop pipeline. We begin by verifying that the latent dependency structure is recoverable from the synthetic continuous traces before any Booleanization is applied. We then examine the Booleanization step itself, focusing on how signal strength, detector threshold, and latent dependency size affect detection quality. Finally, we report the runtime of the main offline stages to assess whether the interpretable model-refresh pipeline remains practical at the slower timescale for which it is intended.

A. Recoverability from continuous traces

Before studying Booleanization, we first ask a simpler question: is the dependency structure visible in the continuous traces at all? To check this, we train one decision tree per KPI to predict discretized ΔK_j from $(\Delta P, P, K)$, and then convert the learned trees into an estimated influence matrix L_{pred} . This serves as a sanity check on the generator: if a simple interpretable model can recover L^* , then the synthetic traces contain the structure we want to study.

Table I summarizes this continuous-trace recoverability step. Recoverability is strong overall, with micro-averaged precision, recall, and F1 all close to 0.98, and an exact-match accuracy of 0.946. This indicates that the latent dependency structure is already well represented in the continuous traces before Booleanization is applied.

The main trend is that overlap affects full-matrix recovery more clearly than edge-wise recovery. In the high-overlap regime, precision, recall, and F1 remain high, but exact-match accuracy drops to 0.908, indicating that denser dependency

patterns are more likely to incur at least one structural mistake even when most individual edges are recovered correctly. By contrast, the sparse regime achieves the highest exact-match accuracy, although its edge-level metrics show larger variability across cases. Overall, these results support the intended role of this step: the continuous data preserve the latent support pattern well enough for a simple interpretable model to recover it, so later errors are more naturally attributed to the Booleanization stage rather than to the generator hiding the structure too well.

B. Detection quality under signal strength, threshold choice, and dependency size

Fig. 3 summarizes the Booleanization step from three complementary viewpoints. Panel (a) studies signal strength, measured by $\Delta P_{\text{step}}/\sigma$, which controls how clearly control-induced KPI responses separate from background variation. Panel (b) studies the detector threshold z_{th} used in (4) to declare a KPI-response event. Panel (c) shows how the same threshold tradeoff behaves across latent dependency structures of different sizes, measured by the number of true parameter-KPI edges in the planted graph. Taken together, these panels distinguish limits imposed by the data itself from limits imposed by detector calibration or by structural complexity.

Panel (a) shows a clear weak-signal to strong-signal transition. At small values of $\Delta P_{\text{step}}/\sigma$, recall is poor because true KPI responses are difficult to separate from noise. As signal strength increases, recall rises sharply and F1 improves with it, while precision is already high and quickly saturates. This indicates that the main challenge in the low-SNR regime is missed detections rather than a large false-positive burden.

Panel (b) shows that threshold calibration provides a transparent operating-point tradeoff. At low thresholds, recall remains high, but precision is poor, which indicates that many background fluctuations are labeled as signal. As the threshold increases, precision rises sharply while recall stays high over much of the range, and F1 correspondingly improves before saturating. This suggests that the Booleanization step is most effective in a moderate-to-high threshold regime, where the detector has become selective without sacrificing much sensitivity.

Panel (c) examines true dependency edges more directly by plotting mean F1 as a function of the number of true parameter-KPI dependency edges for three high detector thresholds, $z_{\text{th}} \in \{4, 4.5, 5\}$. This view focuses on the selective-threshold regime identified in Panel (b), where F1 is close to saturation, and shows whether performance degrades as the planted dependency graph becomes denser. The $z_{\text{th}} = 4.5$ and $z_{\text{th}} = 5$ curves remain near-perfect across the full tested range of graph sizes, while $z_{\text{th}} = 4$ starts lower for very sparse graphs but quickly rises and remains stable above approximately 0.9. Overall, these results suggest that once the detector threshold is sufficiently selective, Boolean event-detection quality is largely stable across the tested range of dependency-graph sizes, with only modest variation at the lowest threshold shown.

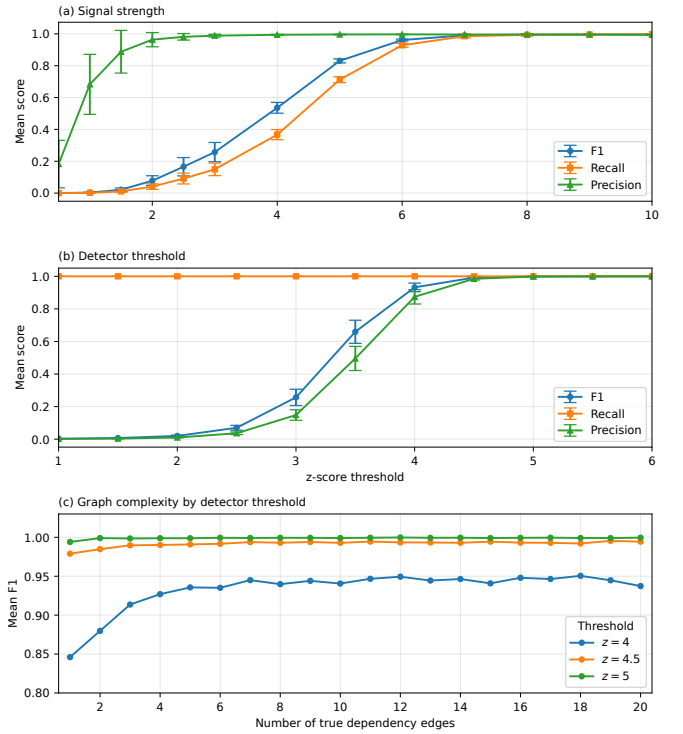


Fig. 3. Detection-quality trends for the binary event-detection step. (a) Mean F1, recall, and precision versus signal strength, measured by $\Delta P_{\text{step}}/\sigma$. (b) Mean F1, recall, and precision versus detector threshold z_{th} . (c) Mean F1 versus the number of true parameter-KPI dependency edges for selected detector thresholds.

Overall, these results show that Booleanization quality is governed first by the separation between control-induced responses and the noise floor, and second by calibration of the detector threshold. Once the signal is sufficiently strong, the remaining task is mainly to choose a threshold that suppresses spurious detections without discarding true events.

C. Runtime analysis

Fig. 4 reports the computational cost of the main offline stages of the proposed slow loop. Panel (a) shows the cost of synthetic trace generation. Panel (b) isolates the downstream slow loop cost excluding generation, separating the decision-tree fit/predict/extract stage from the subtotal of the non-generation learning stages. Panel (c) reports the corresponding Booleanization cost, separating threshold setup from conversion to Boolean events. These results are intended to assess whether the slow loop analysis remains practical at the offline timescale for which it is designed.

Two trends are clear. First, runtime grows predictably with the number of timesteps in all stages. Second, the dominant cost is trace generation, while the added analysis stages remain comparatively small. The learning subtotal in panel (b) stays well below the generation cost in panel (a), and the Booleanization costs in panel (c) are smaller still. In particular, threshold setup and continuous-to-Boolean conversion both re-

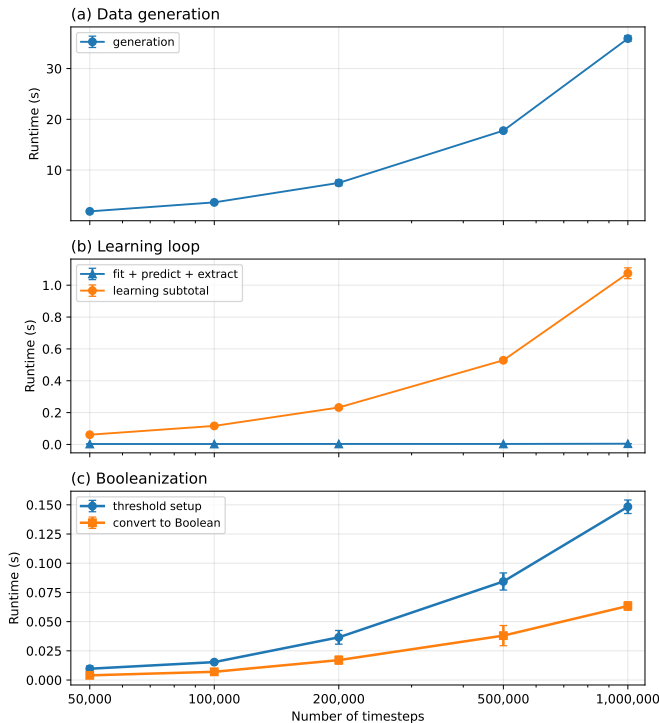


Fig. 4. Runtime breakdown of the main offline stages versus number of timesteps. (a) Data-generation cost. (b) Learning-loop cost excluding generation, showing the decision-tree fit/predict/extract stage and the subtotal of the non-generation learning stages. (c) Booleanization cost, showing threshold setup and conversion to Boolean.

main lightweight over the tested range relative to the upstream data-generation stage.

The main point of this figure is therefore not that these computations should belong in the fast control path. Rather, it is that the interpretable preprocessing needed to refresh the dependency model does not dominate the offline cost. This supports the intended use of the method within a fast/slow architecture: heavier continuous-data processing can remain in the slow loop, while downstream runtime reasoning operates on the resulting compact Boolean dependency representation.

D. Discussion

The results suggest a simple overall picture. First, the continuous traces generated by the simulator do contain the latent dependency structure, so the problem is identifiable under chosen synthetic settings. Second, the Booleanization step exhibits a clear and interpretable operating-point tradeoff: low thresholds favor sensitivity but admit many spurious detections, whereas moderate-to-high thresholds substantially improve F1 by becoming more selective. Third, increasing signal strength mainly improves recall up to saturation, while the overall threshold trend remains similar across latent dependency graphs of different sizes.

An important implication is that the main bottleneck is not simply raw signal strength alone. In the tested regime, stronger signal quickly removes missed detections, but it does

not eliminate a small residual number of false positives. This means that once recall has saturated, further gains are limited less by signal strength than by the detector’s false-positive floor and by the calibration of the significance threshold.

Taken together, these results suggest that the Booleanization step can be effective when the significance threshold z_{th} is chosen appropriately and the control-induced KPI response is sufficiently separated from background variation. The runtime results also indicate that both the learning-loop and Booleanization computations are practical for offline model refresh, with total cost dominated by data generation rather than by the interpretable inference steps themselves. This supports the intended use of the method within a dynamic/learning architecture, in which heavier continuous-data analysis is confined to the slow loop and downstream reasoning operates on the resulting binary dependency representation.

IV. CONCLUSION

This paper studied the problem of learning an interpretable binary parameter–KPI dependency structure for AI-RAN control systems. A central component of the framework is the Booleanization step, which we formulate as a significance-detection problem linking continuous, noisy telemetry to an interpretable dependency model. To support this study, we introduced a synthetic traffic-generation framework with known latent dependencies, enabling controlled evaluation of both dependency recoverability and Booleanization quality.

The experimental results showed that meaningful dependency structure can be recovered when the underlying continuous traces contain sufficient signal, and that the quality of the recovered structure depends strongly on the Booleanization step. In particular, detection performance depends heavily on the availability of null (no-intervention) observations used to estimate the noise baseline. Across the tested generator settings, this factor was more consistently associated with detection quality than signal magnitude or dataset size alone.

These results show that Booleanization quality has a direct impact on the quality of the inferred dependency structure. Poor calibration introduces false activations and missed responses, whereas well-calibrated detection allows even a simple Boolean support-recovery procedure to produce a compact and interpretable dependency representation.

The present study has several limitations. The evaluation is conducted on synthetic data, and the generator models controllers of the feedback-driven, state-reactive type: each control action depends only on the current KPI state rather than on longer histories, learned models, or evolving policies. This design choice is representative of a broad class of O-RAN xApps and rApps, and it yields traces with recoverable structure, but it does not capture the defining characteristic of AI-RAN deployments in which controllers adapt their behavior over time as they accumulate data. Extending the generator and the learning pipeline to handle policy-shifting or model-updating controllers is the primary step needed to move from the foundational setting studied here to a fully AI-RAN-relevant evaluation. Although the current methodology could

in principle accommodate more complex data-generation rules, such extensions would be difficult to validate without access to real AI-RAN telemetry.

Future work will extend this study in four directions. First, we will evaluate the Booleanization framework under a broader family of synthetic generators and more realistic AI-RAN-inspired control settings, including controllers that update their policies over time. Second, we will investigate streaming variants of the method for tracking time-varying dependency structure, which is essential when controller behavior or network conditions shift. Third, we will study how the recovered Boolean dependency matrix can support downstream tasks such as conflict monitoring and mitigation. Fourth, we will pursue validation on real or high-fidelity AI-RAN/O-RAN traces to assess how well the pipeline transfers from the synthetic setting to operational deployments.

REFERENCES

- [1] 3GPP, “NG-RAN; Architecture Description,” 3rd Generation Partnership Project (3GPP), Technical Specification TS 38.401, 2026, release 19, version 19.2.0. Accessed: May 13, 2026. [Online]. Available: <https://portal.3gpp.org/desktopmodules/Specifications/SpecificationDetails.aspx?specificationId=3219>
- [2] A. S. Abdalla, P. S. Upadhyaya, V. K. Shah, and V. Marojevic, “Toward next generation open radio access networks: What o-ran can and cannot do!” *IEEE Network*, vol. 36, no. 6, pp. 206–213, 2022.
- [3] M. Polese, L. Bonati, S. D’Oro, S. Basagni, and T. Melodia, “Understanding o-ran: Architecture, interfaces, algorithms, security, and research challenges,” *IEEE Communications Surveys & Tutorials*, vol. 25, no. 2, pp. 1376–1411, 2023.
- [4] O. S. Community, “O-RAN architecture overview,” [Online]. Available: <https://docs.o-ran-sc.org/en/latest/architecture/architecture.html>, 2026, accessed: May 13, 2026.
- [5] C. Adamczyk and A. Kliks, “Conflict mitigation framework and conflict detection in o-ran near-rt ric,” *IEEE Communications Magazine*, vol. 61, no. 12, pp. 199 – 205, 2023.
- [6] P. Brach del Prever, S. D’Oro, L. Bonati, M. Polese, M. Tsampazi, H. Lehmann, and T. Melodia, “Pacifista: Conflict evaluation and management in open ran,” *IEEE Transactions on Mobile Computing*, vol. 24, no. 10, pp. 10 590 – 10 605, 2025.
- [7] A. E. Giannopoulos, S. T. Spantideas, G. Levis, A. S. Kalafatis, and P. Trakadas, “Comix: Generalized conflict management in o-ran xapps—architecture, workflow, and a power control case,” *IEEE Access*, vol. 13, pp. 116 684 – 116 700, 2025.
- [8] A. Zolghadr, J. F. Santos, L. A. Dasilva, and J. Kibilda, “Learning and reconstructing conflicts in o-ran: A graph neural network approach,” 2025.
- [9] M. Al Shami, J. Yan, and E. T. Fapi, “O-ran xapps conflict prediction using graph convolutional networks,” *IEEE Transactions on Mobile Computing*, 2026.
- [10] S. Montebugnoli, A. Sabbioni, F. Callegati, L. Foschini, and P. Bellavista, “CLO5ER: A composable lightweight observability for 5G RAN environment inside Near-RT RIC,” 2025, pp. 1900 – 1905.
- [11] I. Lindra, Hendrawan, A. Subekti, and E. Mulyana, “Integration of artificial intelligence into radio access network (ai-ran): Architecture, classification, and development focus,” 2025.
- [12] C. Djidjev and N. Kaminski, “Runtime dependency tracking in AI-RAN using Boolean matrix inference,” 2026, arXiv preprint. [Online]. Available: <https://arxiv.org>
- [13] V. S. Borkar, “Stochastic approximation with two time scales,” *Systems & Control Letters*, vol. 29, no. 5, pp. 291–294, 1997.
- [14] V. R. Konda and J. N. Tsitsiklis, “Convergence rate of linear two-time-scale stochastic approximation,” *The Annals of Applied Probability*, vol. 14, no. 2, pp. 796–819, 2004.
- [15] P. V. Kokotovic, H. K. Khalil, and J. O’Reilly, *Singular Perturbation Methods in Control: Analysis and Design*, ser. Classics in Applied Mathematics. Philadelphia, PA: Society for Industrial and Applied Mathematics, 1999, vol. 25.
- [16] D. B. Neill and G. F. Cooper, “A multivariate bayesian scan statistic for early event detection and characterization,” *Machine Learning*, vol. 79, no. 3, pp. 261 – 282, 2010.
- [17] C. Truong, L. Oudre, and N. Vayatis, “Selective review of offline change point detection methods,” *Signal Processing*, vol. 167, 2020.
- [18] R. Baragona and F. Battaglia, “Outliers detection in multivariate time series by independent component analysis,” *Neural Computation*, vol. 19, no. 7, pp. 1962 – 1984, 2007.
- [19] M. A. Belay, S. S. Blakseth, A. Rasheed, and P. Salvo Rossi, “Unsupervised anomaly detection for iot-based multivariate time series: Existing solutions, performance analysis and future directions,” *Sensors*, vol. 23, no. 5, 2023.
- [20] C.-H. Zhao and X. Chen, “From the decomposition perspective: A survey of industrial time series modeling and process monitoring based on multivariate statistical methods,” *Kongzhi yu Juece/Control and Decision*, vol. 39, no. 11, pp. 3521 – 3546, 2024.
- [21] G. Andrienko, N. Andrienko, M. Mladenov, M. Mock, and C. Poelitz, “Extracting events from spatial time series,” 2010, pp. 48 – 53.
- [22] X. Zhou, C. Brif, and I. Lourentzou, “mtsbench: Benchmarking multivariate time series anomaly detection and model selection at scale,” *Transactions on Machine Learning Research*, vol. 2026 February, 2026.
- [23] Y. Cheng, Z. Wang, T. Xiao, Q. Zhong, J. Suo, and K. He, “CausalTime: Realistically generated time-series for benchmarking of causal discovery,” in *International Conference on Learning Representations*, 2024. [Online]. Available: <https://openreview.net/forum?id=iad1yyGme>